 CMC, vol.51, no.1, pp.43-62, 2016

Molecule Dynamics Study on Heat Transfer at Gas-Nanoparticle Interface

ZichunYang[1], Gaohui Su[1,2], Bin Chen[1]

Abstract: The molecular dynamics (MD) simulations were used to understand the heat transfer process between the gas phase and the solid skeleton in the nanoporous silica aerogels. The amorphous silica nanoparticles were generated by the MD simulations and the energy accommodation coefficient (EAC) between the gases and the nanoparticles was calculated based on the results of the non-equilibrium molecular dynamics (NEMD) simulations. The apparent thermal conductivity (ATC) of the gases between the heat source and heat sink was also obtained. The effects of the temperature, the particle diameter and the molecule type on the EAC and the ATC were investigated. The results indicate that the EAC decreases with the increase of temperature within the calculating range. When the preset temperature is constant, the EAC increases with the increasing of the particle diameter and eventually approaches a specific value. When the preset temperature is 300 K and the particle size is 4 nm, the obtained EAC for the N_2 gas and the O_2 gas is close to each other and both are less than that of the Ar gas. The results also indicate that the heat transferred through the gas-nanoparticle interface is far less than that through the neighbouring nanoparticles in silica aerogels.

Keywords: Energy accommodation coefficient; Molecular dynamics; Nanoparticle; Amorphous silica.

1 Introduction

Silica aerogels are typical nanoporous materials with open pores and network structure, they have unique properties such as high porosity, high specific surface area, low thermal conductivity, low dielectric constant and low refractive index [Aegerter, Leventis, and Koebel (2011); Dorcheh and Abbasi (2008)]. Because of their unique structural and physicochemical properties, silica aerogels have broad application prospects in many areas, especially as a super thermal insulating material

[1] Naval University of Engineering, 430033, China
[2] Corresponding author: su_gaohui@163.com

in the energy field owing to the prominent natures such as lightweight, high temperature resistance, non-flammability and low thermal conductivity [Fricke, Heinemann, and Ebert (2008)]. It is of important engineering value to study the internal heat transfer mechanism to further optimize the thermophysical properties of the material, its across-scale structure also provides an excellent research object for the multi-heat transfer process.

The specific surface area of the aerogels is about $600\sim1200\ m^2\cdot g^{-1}$, which greatly increases the interface between the gas phase and the solid skeleton. Thus, when the gas molecules move in the pores, the chance for the molecules to collide with the solid skeleton is much larger than that for them to collide with each other. This decreases the energy exchange between the gas molecules and increases the energy exchange between the gas phase and the solid skeleton. The heat conduction between the gas and the skeleton increases the complexity of the heat transfer in nanoporous materials. Understanding the energy transport process between the gas phase and the solid skeleton is the precondition to establish the heat conduction model for nanoporous materials [Coquard, Baillis, Grigorova, Enguehard, Quenard, and Levitz (2013)].

The pore size of the aerogels is distributed between $1\sim100$ nm which is comparable to the mean free path (MFP) of the air molecules at ambient conditions. When the MFP of the gas molecules is comparable with the characteristic scale, the rarefied gas effect is obvious and a temperature jump occurs at the interface between the gas and the solid surface, which results in a thermal boundary resistance [Zhang (2007)]. The energy accommodation coefficient (EAC) is a measure for characterizing the efficiency of kinetic energy exchange between the gas molecules and the wall atoms and can be used to determine the thermal boundary resistance as well as the temperature jump at the interface[Sun and Li (2009); Liang, Evans, and Keblinski (2013)]. The key to understand the energy transfer process between the gas molecules and solid surface lies in the determination of the EAC.

Although the concept of EAC has been introduced and investigated more than one century, there is no quantitative theory to determine the accurate value, only some empirical models are available which need to be confirmed with experimental data [Liang and Keblinski (2014)]. Since many factors can affect the EAC, such as the mass of the gas molecules and the wall atoms, the strength of interaction potential between the gas molecules and the wall atoms, the temperature and so on, it is difficult to study the effect of an independent factor only by experimental measurements.Currently, molecular dynamics (MD) simulations play an important role in understanding the behavior of nanoscale systems as the computing performance increases [Namilae, Chandra, Srinivasan, and Chandra (2007); Tu, Lee, Zhang, and Li (2014)]. More and more researchers begin to use MD simulations to investigate

the interaction between the gas and the solid surface. Sun calculated the EAC of argon gas between two platinum plates using a two-dimensional non-equilibrium molecular dynamics (NEMD) simulation [Sun and Li (2009)]. Schiffres predicted the EAC between various gases and single-walled carbon nanotubes using MD simulations [Schiffres, Kim, Hu, McGaughey, Islam, and Malen (2012)] and the calculated EAC confirmed the poor energy exchange during the collisions. Lin calculated the EAC between noblegases and carbon nanotubes using the same MD method, the results show that the EAC increases as the carbon nanotube diameter increases, and eventually approaches the EAC between gases and graphite [Lin and McGaughey (2013)]. Liang studied the effect of interfacial parameters on the EAC using MD simulations [Liang and Keblinski (2013)]. Liang also studied the effect of functionalizing solid surface with organic self-assembled monolayers on the heat exchange efficiency between a solid and a gas by MD simulations [Liang, Evans, Desai, and Keblinski (2013)]. The above references mainly focus on the interaction between gases and solid surface. Choi calculated the EAC between the He gas and nanometer-sized Ar or N_2 particles using MD simulations [Choi, Yi, Lee, and Lee (2012)], but they haven't investigated the effect of the particle size on the EAC. In this work, amorphous silica nanoparticles were generated using the MD simulations and the effects of particle size, temperature and molecule types on the interaction between the gas and nanoparticle were investigated based on the NEMD simulations.

2 Method

2.1 MD model

2.1.1 Physical model

Silica aerogel skeletons are composed of interconnected nanometer-sized particles. To reduce the amount of calculation, the interaction between gas molecules and one amorphous silica particle is studied in this paper. NEMD method was used to simulate the interaction processes. The physical model was shown in Figure 1. The simulation domain was a cubic box with side length $L = 20$ nm. The nanoparticle was settled at the center of the simulation box and the remainder space in the box was filled with gas molecules. During the NEMD simulation, part of the particle region was set as the heat source, and the region away from the particle and near the box boundary was set as the heat sink, as is shown in Figure 2. The heat of $+$Q was applied to the Si and O atoms within the region of the heat source and the heat of $-$Q was applied to the gas molecules within the region of the heat sink to establish a non-equilibrium state of the system, where "$+$" indicates adding heat and "$-$" indicates removing heat. In order to prevent the overall movement of the

particle, the atoms in the central region of the particle were frozen. The rest atoms in the particle keep doing thermal motion and were set as the heat source.

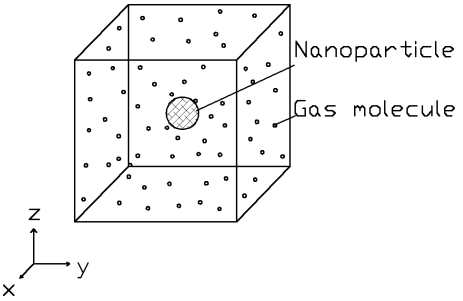

Figure 1: Configuration of the nanoparticle and the gas molecules in the simulation box.

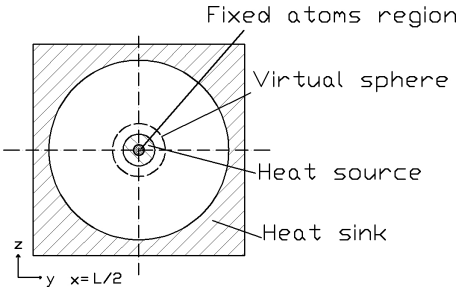

Figure 2: Configuration of the computing region in the NEMD simulation.

2.1.2 Interatomic potential

The interaction between the atoms in the simulation system is described by the interatomic potential which determines the fundamental properties of the material. Selecting an appropriate interatomic potential is the key for MD simulations and is directly related to the accuracy of the calculating results.

(1) Interatomic potential for atoms composing the nanoparticle

The material of the nanoparticle is amorphous silica. Based on the BKS interatomic potential, Jund calculated the thermal conductivity of vitreous silica using NEMD method and the results were in good agreement with the experimental data at temperature above 20 K [Jund and Jullien(1999)]. Yoon calculated the thermal conductivity of the crystalline α- and β-quartz in high-temperature range using NEMD simulations and BKS interatomic potential, the results were also in agreement with experiment data [Yoon, Car, and Srolovitz (2004)]. Mahajan calculated the thermal conductivity of amorphous silica nanoparticles and nanowires using the MD simulations and BKS interatomic potential [Mahajan and Subbarayan (2007)]. Huang calculated the thermal conductivity of crystalline and amorphous silica films using NEMD simulation and BKS interatomic potential [Huang, Tang, Yu, and Bai (2009)]. Thomas predicted the thermal conductivity of amorphous nanoporous silica using NEMD simulation and BKS interatomic potential [Thomas, Jin, and Laurent (2011)]. These calculated results demonstrate that the BKS interatomic potential can accurately capture the transport behavior of silica materials. Therefore, in this work, the BKS potential was selected to model the interaction of atoms in the nanoparticle. It is a two-body potential and is given by Van Beest, Kramer

and Van Santen (1990):

$$u(r_{ij}) = \frac{q_i q_j}{r_{ij}} + A_{ij}\exp(-B_{ij}r_{ij}) - \frac{C_{ij}}{r_{ij}^6} \tag{1}$$

Where, q_i is the charge of atom i. The charges of Si and O are $+2.4$ e and -1.2 e, respectively. A_{ij}, B_{ij}, C_{ij} are constants specified for the particular types of atoms i and j. Their values are listed in Table 1, which are proposed by Van Beest, Kramer, and Van Santen (1990).

Table 1: BKS Parameters for the interatomic interaction in the nanoparticle.

Pairs	A_{ij}/eV	B_{ij}/Å^{-1}	C_{ij}/eV
Si-Si	0.0000	0.0000	0.0000
O-O	1388.7330	2.76000	175.0000
Si-O	18003.7572	4.87318	133.5381

In equation (1), the Coulombic term is a long-range interaction and cannot be solved directly. The commonly used method is Ewald summation, in which the calculation of energy is performed in two parts: the real-space part and the part in Fourier space. Short-range force is calculated in the real space and long-range force is calculated in the Fourier space [Frenkel and Smit (2002)]. However, this method needs a large amount of computation. Here, the Wolf method was used to handle the Coulombic term which needs relatively small amount of computation and can also meet the requirements of accuracy [Wolf, Keblinski, Phillpot, and Eggebrecht (1999); Mahajan and Subbarayan (2007)]. The wolf method is given by equation (2):

$$\frac{q_i q_j}{r_{ij}} \approx \frac{q_i q_j \operatorname{erfc}(\alpha r_{ij})}{r_{ij}} \tag{2}$$

Where α is the damping parameter; $\operatorname{erfc}(\alpha r) = 1 - \operatorname{erf}(\alpha r)$, $\operatorname{erf}(\alpha r)$ is error function:

$$\operatorname{erf}(\alpha r) = \frac{2}{\sqrt{\pi}} \int_0^{\alpha r} \exp\left(-t^2\right) dt \tag{3}$$

(2) Gas molecules model

The gases simulated in this work are Ar, O_2, and N_2. Among them, Ar is a monatomic molecule, O_2 and N_2 are diatomic molecules. The covalent N-N and O-O bonds are modeled by Morse potential [Nasrabadi and Foroutan (2012)]:

$$U(r_{ij}) = \varepsilon_0 \left[1 - e^{-k\left(r_{ij} - r_0\right)}\right]^2 \tag{4}$$

Where ε_0 determines the depth of the potential well, k is the stiffness parameter, r_0 is the equilibrium bond distance. The values of these parameters for O_2 and N_2 are listed in Table 2.

Table 2: Morse parameters for the covalent bonds.

Bonds	ε_0/eV	k/Å^{-1}	r_0/Å
N-N	9.7680	2.642	1.098
O-O	5.1190	2.680	1.207

(3) Interatomic potential for atoms in different molecules

Both the interaction for atoms in different gas molecules and the interaction between the atoms composing the gas molecules and the atoms composing the nanoparticles are modeled by the well known 12-6 Lennard-Jones (L-J) interatomic potential:

$$U_{\mathrm{LJ}}(r_{ij}) = 4\varepsilon\left[\left(\frac{\sigma}{r_{ij}}\right)^{12} - \left(\frac{\sigma}{r_{ij}}\right)^{6}\right] \tag{5}$$

The 12-6 LJ parameters are listed in Table 3.The N_2-O (in silica), N_2-Si, O_2-O (in silica) and O_2-Si interaction parameters were calculated by the Lorentz-Berthelot mixing rules [Allen and Tildesley (1987)]:

$$\sigma_{\mathrm{ab}} = \frac{1}{2}(\sigma_{\mathrm{a}} + \sigma_{\mathrm{b}}) \tag{6}$$

$$\varepsilon_{\mathrm{ab}} = \sqrt{\varepsilon_{\mathrm{a}}\varepsilon_{\mathrm{b}}} \tag{7}$$

Where the subscript a and b represent different types of atoms.

Table 3: Lennard-Jones parameters for the intermolecular interactions.

Atom	σ/Å	ε/eV	Reference
N (in N_2)	3.68	7.90×10^{-3}	Nasrabadi
Ar (in Ar)	3.40	10.61×10^{-3}	Lin
O (in O_2)	3.43	9.75×10^{-3}	Nasrabadi
Si (in SiO_2)	3.39	25.37×10^{-3}	Malek
O (in SiO_2)	3.00	19.81×10^{-3}	Yoshioka

2.1.3 Simulation procedure and details

The main simulation process includes four steps: (1) Generation of the amorphous silica nanoparticle. (2) Addition of gas molecules into the simulation box. (3) NEMD simulation of the heat transfer process. (4) Post-treatment of the simulation results. The calculation was implemented by the Large-scale Atomic/Molecular Massively Parallel Simulator (LAMMPS) [Plimpton (1995)].

(1) Generation of the amorphous silica nanoparticle

In this paper, the amorphous silica materials were generated by a melting-quenching procedure similar to that described by Mahajan and Subbarayan (2007); Thomas, Jin, and Laurent (2011). The α-cristobalite was first heated to liquid state and then quenched to amorphous solid state. The BKS potential is a good description of the interaction between atoms in silica materials, however, in the simulation of the melting process, the temperature is very high and the atomic motion is very intensive so the atoms may be very close to each other. The BKS potential cannot provide enough repulsive forces to separate them and the error of missing atoms would occur. To solve this problem, a 24-6 LJ interatomic potential was added to the BKS potential in the melting-quenching processes. The modified interatomic potentialis given by equation (8) and the parameters for 24-LJ interatomic potential are listed in Table 4:

$$u(r_{ij}) = \frac{q_i q_j}{r_{ij}} + A_{ij}\exp(-B_{ij}r_{ij}) - \frac{C_{ij}}{r_{ij}^6} + 4\varepsilon_{ij}\left[\left(\frac{\sigma_{ij}}{r_{ij}}\right)^{24} - \left(\frac{\sigma_{ij}}{r_{ij}}\right)^{6}\right] \tag{8}$$

Table 4: Parameters for 24-6 LJ potential.

Pairs	ε/eV	σ/Å
Si-Si	13.20	0.40
O-O	4.78×10^{-4}	2.20
Si-O	1.12×10^{-2}	1.35

During the generation process of the amorphous silica, periodic boundary conditions were applied in all directions and the velocity-verlet integrator was used to update the position and velocity of the atoms in the system. The selection of time step is very important. If the time step is too small, it would need a lot of time to simulate a process, if the time step is too large, it may lose the calculating accuracy. Here, the time step is set to 0.905 fs which is similar to that in the reference [Thomas, Jin, and Laurent (2011)].

The generation process of the nanoparticle consists of four steps. The first step is melting. The established α-cristobalite model was heated at a temperature of 5000

K using the Nose-Hoover thermostat for 60000 time steps [Nosé (1984); Hoover (1985)]. Then the solid material was melted to liquid state. The second step is quenching using the NPT ensemble. The system temperature was gradually decreased from 5000 K to 300 K for 1500000 time steps and the cooling-rate was 3.45×10^{12} K·s^{-1} which is much larger than that is required for amorphous silica generation. The third step was isotropic expanding of the system. When the system was quenched using the NPT ensemble, the system size reduces in all dimensions and the density of the obtained material is 2518 kg·m^{-3} which is higher than the typical value of the amorphous silica. Therefore, after the quenching step, the system was expanded in all dimensions. After adjustment, the final density is about 2175 kg·m^{-3}. Figure 3 is the radial distribution function (RDF) of the generated amorphous silica. As can be seen, the calculated RDF is consistent with the typical RDF forms of the amorphous material. Within a small range, the RDF fluctuates as the radius increases and at a long distance, it gradually approaches 1. The first peak position is 1.62 Å which is in good agreement with the reported value, 1.64 Å [Kittel (2005)]. The final step was deleting atoms. The obtained material model is cubic so some atoms should be deleted to form a sphere nanoparticle. The generated amorphous silica nanoparticle was shown in Figure 4.

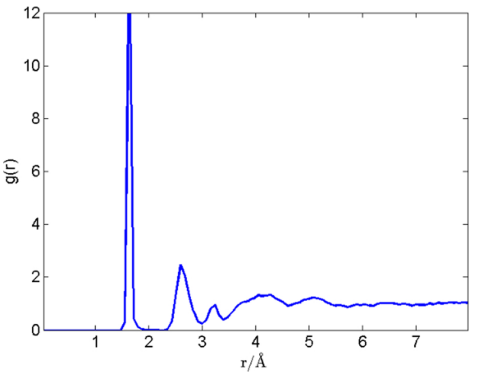

Figure 3: Dependence of the radial distribution function of the generated amorphous silica versus the radius.

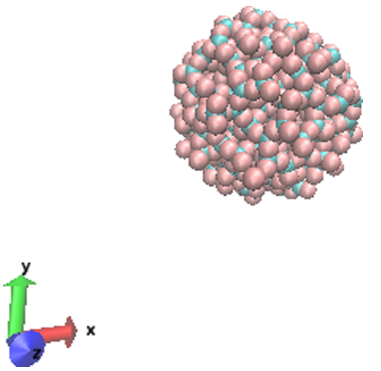

Figure 4: The atomic model of a generated amorphous silica nanoparticle.

(2) Adding gas molecules into the simulation box

The number of gas molecules added to the box was determined by the pressure, temperature and the volume of the gas region. It can be calculated by the following equation:

$$N_g = \frac{PV_gN_A}{RT} \tag{9}$$

Where N_g is the number of the gas molecules, $R$is the universal gas constant and $R = 8.314$ J·(mol·K)$^{-1}$, N_A is Avegadro's constant and $N_A = 6.022 \times 10^{23}$ mol^{-1}, V_g is the volume of the gas region, it was determined by the volume of the simulation box and the volume of the nanoparticle:

$$V_g = L^3 - \frac{4}{3}\pi r_{\mathrm{p}}^3 \tag{10}$$

Where r_p is the radius of the nanoparticle. To obtain a better statistical result, the pressure was set as 5 atm, higher than the ambition pressure, so that more gas molecules can be tracked in once simulation. Meanwhile, the temperature T in equation (9) was set as 300 K. In this case, the number density of the gas molecules was kept a constant in different simulations. Thus N_g is only determined by the size of the nanoparticle. Figure 5 is an atomic model of the system after adding O_2 molecules

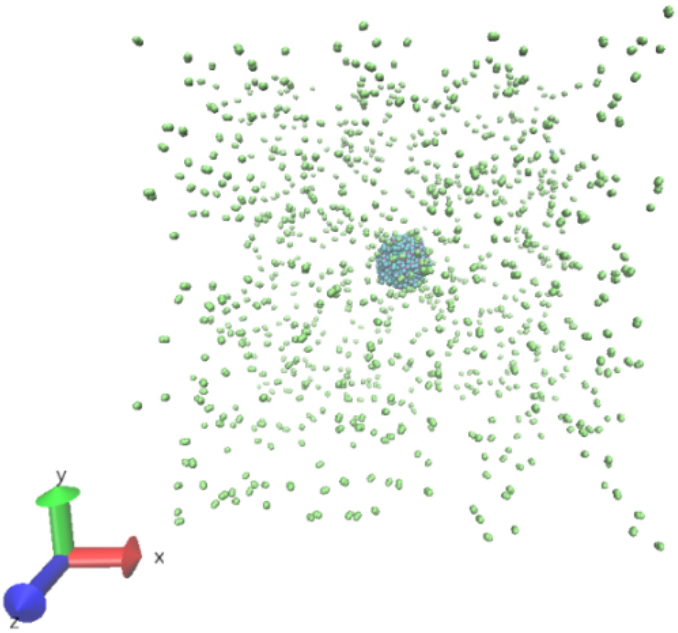

Figure 5: An atomic model of the system after adding gas molecules.

(3) NEMD simulation

During the NEMD simulation of the heat transfer between nanoparticle and the gases, the velocity-verlet integrator and periodic boundary conditions were also applied. As previousely described, the selection of time step is very important.

Usually, the time step selected is less than one-tenth of the fastest movement period in the system. According to the kinetic theory, the lighter the gas molecule is, the faster the molecule moves. Therefore, the O_2 and N_2 molecules are faster than the Ar molecule. Nasrabadi investigated the adsorption of a N_2-O_2 mixture on carbon nanotube bundles using MD simulations and the time step is 1 fs [Nasrabadi and Foroutan (2012)]. Mahajan predicted the thermal conductivity of amorphous silica using MD simulations and the time step is 1 fs [Mahajan and Subbarayan (2007)]. Yoon calculated the thermal conductivity of crystalline quartz using MD simulations and the used time step is 0.97 fs [Yoon, Car, and Srolovitz (2004)]. According to these references, the time step used here for the NEMD simulations was 1 fs.

After adding gas molecules in to the simulation box, the system was at a state far from equilibrium. If the simulation is directly run, there may be an error that an ultra-high temperature appears and some atoms would be blown out of the simulation box. Therefore, an energy minimization procedure must be executed to relax the system at first.

After the energy minimization procedure, the atoms in the fixed atoms region werefrozen by the following method. Their initial velocities were set as zero and the forces applied on them by other atoms were kept zero in the following simulation. Thus, the coordinates of these fixed atoms will remain unchanging and the rest moving atoms would be still influenced by the fixed atoms and the overall position of the nanoparticle would be relatively fixed. Then the system was equilibrated to a preset temperature T_{pre} using the Nose-Hoover thermostat and running 20 000 time steps under the NVT ensemble. Figure 6 shows the dependence of the system temperature versus the time steps during the pre-equilibrate process. The diameter of the nanoparticle was 4 nm and the gas was O_2. The preset temperature was 300 K. It can be seen that the system temperature reaches the preset temperature in 1000 time steps and then fluctuates around it. In our calculation, the system temperature T_{sys} refers to the temperature of the collection of the moving atoms and it was calculated by the equation (11) [Chen (2005)]:

$$T_{\text{sys}} = \frac{1}{3N_m k_B} \sum_{i=1}^{N_m} m_i v_i^2 \tag{11}$$

Where N_m is the number of the moving atoms, excluding the fixed atoms, k_B is the Boltzmann's constants and $k_B = 1.381 \times 10^{-23}$ J·K^{-1}, m_i and v_i are the mass and velocity of atom i.

After the pre-equilibrating procedure, the Nose-Hoover thermostat was eliminated and the heat was added/removed to the heat source/sink. The heat transfer rate was 1.602×10^{-9} W. Figure 7 shows the dependence of the temperature versus the

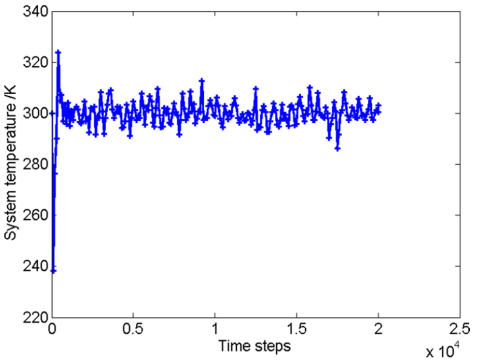

Figure 6: Dependence of the system temperature versus the time steps during the pre-equilibrating process.

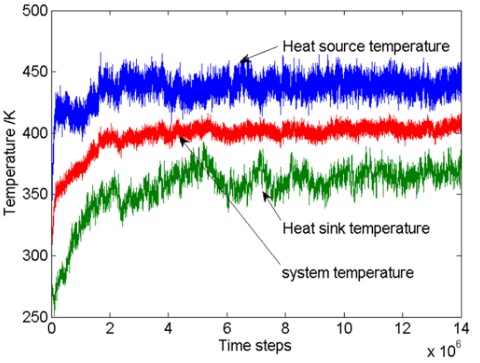

Figure 7: Dependence of the temperature versus the time steps after applying heat on the heat source and the heat sink.

running time steps after applying heat to the heat source and heat sink. It can be seen that the temperature of the heat source, the heat sink and the system increases at the beginning and then approachesthe specific values as the simulation proceeds, indicating the heat transfer reaches the steady state. The running time steps after applying heat was 14 000 000 or 15 000 000 in the following simulations for different system configurations. After the heat transfer process reaches the steady state, the trajectory of the gas molecules and the thermodynamic information of the system were collected for the calculating of the EAC and the ATC.

2.2 EAC calculating

The definition of EAC is given by the equation (12) [Borisov, Litvinenko, Semenov, and Suetin (1978)]:

$$\alpha_E = \frac{E_\mathrm{i} - E_\mathrm{r}}{E_\mathrm{i} - E_\mathrm{w}} \tag{12}$$

Where E_i is the energy brought in by the incident molecules, E_r is the energy carried away by the reflected molecules and E_w is the energy which would be carried away by the reflected molecules if they reached the wall temperature. Amonatomic gas molecule has three degrees of translational freedom. According to the equipartition theorem [Chen (2005)], each freedom contributes energy of $k_BT/2$. Therefore, the E_w for a monatomic gas molecule is $3k_BT_w/2$, where T_w is the wall temperature. For diatomic molecules, there are three degrees of translational freedom, two degrees of rotational freedom and one degree of vibrational freedom. The total energy is the sum of the translational, rotational and vibrational energy. The characteristic temperature for vibrational freedom is usually very high, which is 3390 K for N_2

and 2278 K for O_2 [Zhang (2007)]. In this work, the simulation temperatures were much lower than the characteristic temperatures for vibration freedom, so the contribution of the vibrational mode to the total energy was negligible. Therefore, the E_w for a diatomic gas molecule is $5k_BT_w/2$.

To determine the EAC, a virtual sphere was set outside the nanoparticle. The distance from the surface of the nanoparticle to the virtual sphere was 10 Å which is equal to the cut-off radius of the interatomic potential at the interface. When a gas molecule enters the virtual sphere, the forces are applied by the particle atoms and an incident event occurs; after it moves out of the virtual sphere the forces begins to disappear and a reflected event occurs. The incident event and the reflected event constitute a collision event.

During the NEMD simulation the kinetic energy and the coordinates of the atoms and the thermodynamic properties were output at specific time steps for the post-processing. For the diatomic gas molecules, their mass centers were firstly calculated by the coordinates of the atoms composing those molecules, then the mass center were used to determine whether the molecules are in the virtual sphere or not. The energy of a diatomic molecule was the sum of the kinetic energy of the atoms composing that molecule. For the monatomic gas molecules, the coordinates of the gas molecules were directly used to determine its distance from the particle surface.

When outputting the trajectory of the molecules, attention must be paid to the selection of the output time interval. If the output interval is too small and too frequently, the memory requirement and the storage requirement in the post-processing would increase dramatically. If the output interval is too large, some collision events may be lost. The average speed of the gas molecules doing thermal motion is related to their mass and the temperature and can be estimated by $v = \sqrt{3k_BT/m}$. Among the gases of Ar, N_2 and O_2, N_2 is the lightest and moves the fastest. At the temperature of 300 K, the estimated speed of the N_2 is 516.83 $m{\cdot}s^{-1}$. Here the output interval was set as 0.1 ps. Thus the average distance between sequent sampling instants is about 0.5 Å which ismuch less than the distance between the virtual sphere and the nanoparticle surface. A time interval of 0.1 ps can appropriately balance the requirements of the calculating power and the calculating accuracy.

For each collision event, an instantaneous EAC can be calculated by equation (12). And averaging all the instantaneous EAC would obtain an effective EAC. However, the definition of the EAC by equation (12) has a potential flaw when the incident energy E_i approximates to the wall temperature E_w [Sun and Li (2009); Goodman and Wachman (1976)]. The denominator approaches zero and the singularity occurs. To handle this problem, the collision event in which E_i approximates to E_w were deleted when calculating the effective EAC. The exclusion criterion is given

by equation (13).

$$\frac{|E_{\text{in}} - E_{\text{w}}|}{E_{\text{w}}} < 0.01 \tag{13}$$

Figure 8 shows the variation of the effective EAC versus the averaging time steps of the nanoparticle-O_2 system and the diameter of the nanoparticle is 4 nm, the preset temperature is 300 K. It can be seen that the collision events increase and the effective EAC approximates to a stable value, 0.31 ± 0.03 as the averaging time steps increase.

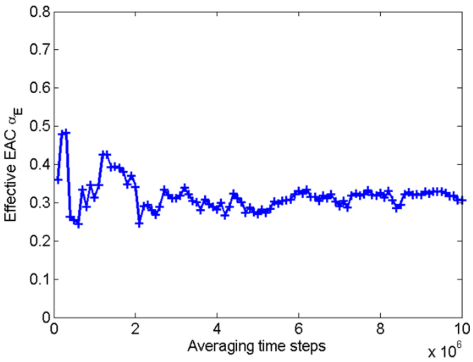

Figure 8: Dependence of effective EAC versus the averaging time steps.

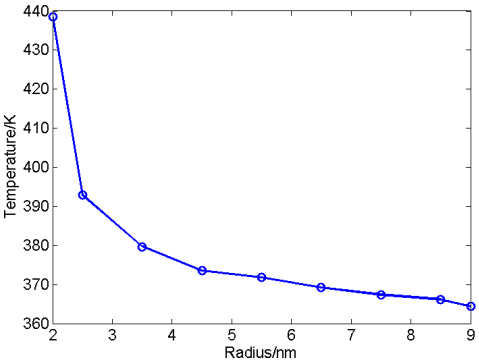

Figure 9: Temperature distribution along the radial direction.

2.3 ATC calculating

As can be seen from Figure 2, the heat transfer region between the heat source and the heat sink is a spherical shell. After reaching the steady state, the heat transfer process between the heat source and heat sink can be seen as a one-dimensional heat conduction problem along the radial direction in the spherical coordinate system. Figure 9 is the temperature distribution along the radial direction. The ATC between the heat source and the heat sink is given by equation (14):

$$\lambda = \frac{\Phi\,(1/r_1 - 1/r_2)}{4\pi\,(T_{\text{hot}} - T_{\text{cold}})} \tag{14}$$

Where r_1 is the radius of the interface between the nanoparticle and the gas region, r_2 is the radius of the interface between the heat transfer region and the heat sink region, T_{hot} is the temperature of heat source and T_{cold} is the temperature of the heat sink.

3 Results and discussion

3.1 Influence of the temperature

Figure 10 shows the dependence of the effective EAC versus the preset temperatures of the nanoparticle-Ar systems. The diameter of the nanoparticle was 4 nm. As can be seen in Figure 10, the EAC decreases with the increasing temperature. Borisov investigated the EAC for the gases He, Ne, Ar and Xe on a Pt surface with experiments and observed a monotonic increase of the EAC with reduction in temperature for all gases, which is in agreement with our simulation results [Borisov, Litvinenko, Semenov, and Suetin (1978)].

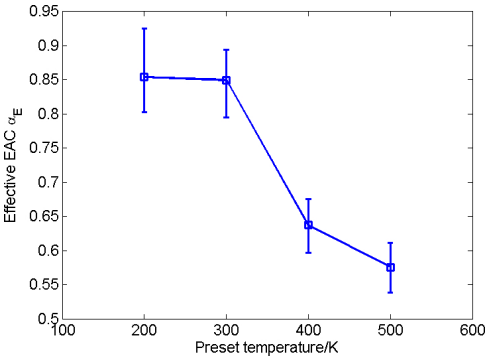

Figure 10: Dependence of the effective EAC versus the preset temperature.

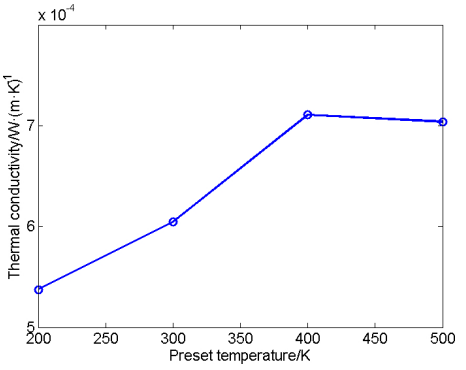

Figure 11: Dependence of the ATC versus the preset temperature.

Figure 11 shows the dependence of the ATC between the heat source and the heat sink versus the preset temperatures. As can be seen , when the preset temperature is 300 K, the ATC is about 6.044 $\times$ 10^{-4} W·(m·K)$^{-1}$. The average temperature of the gas in the heat transfer region is about 330 K. At this termperature, the thermal conductivity of Ar gas in free space is about 1.919 $\times$ 10^{-2} W·(m·K)$^{-1}$ [Touloukian (1970)].The former is far less than the latter and the reason is that the distance between the heat source and the heat sink is 7 nm which is far less than the MFP of the Ar molecules in the free space which is about 76 nm. The heat transfer process was in the free molecule region and the chance for molecules to collide with the heat source is much larger than that for them to collide with each other. The main factor that affects the heat transfer rate is the thermal boundary conductance, h [Lin and McGaughey (2013)]:

$$h = \frac{f k_B N \alpha_E}{2 - \alpha_E} \tag{15}$$

Where N is the gas collision rate on the solid surface per unit area, $f = 4$ for a monatomic gas and $f = 6$ for a diatomic gas. In the simulations, the number density of the gas molecules was constant, so the collision rate is mainly influenced by the speed of the molecules. Therefore, the heat transfer rate is mainly determined by the speed of the molecules and the EAC. It can be seen in figure 11 that the ATC increase slightly as the temperature increases. As the temperature increases, the speed of the molecules increases, resulting in an increase of the ATC. However, the EAC would decrease as the temperature increases which results in a decrease of the ATC. The variation of the ATC versus the preset temperature is the combination of these two influences. The thermal conductivity through the nanoparticles in silica aerogels is on the order of magnitudes of 10^{-1} W·(m·K)$^{-1}$ [Su, Yang, and Sun (2014)] which is much larger than the ATC calculated in this work. Thus it can be concluded that the heat transferred through the neighbouring nanoparticles is much larger than the heat transferred through the gas-nanoparticle interface.

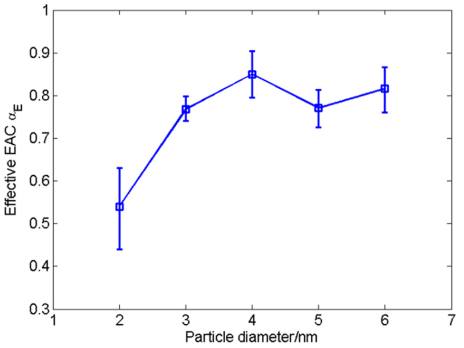

Figure 12: Dependence of effective EAC versus the nanoparticle diameter.

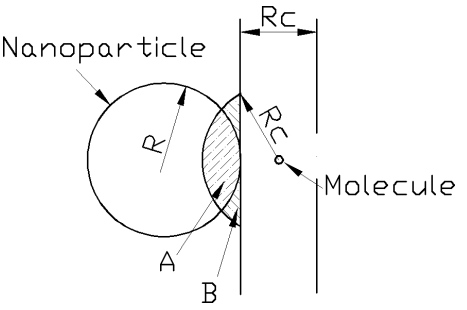

Figure 13: Schematic diagram of the interaction between the nanoparticle and a gas molecule.

3.2 Influence of the particle diameter

Fig. 12 shows the dependence of the effective EAC versus the particle diameter of the nanoparticle-Ar systems. The preset temperatures were 300 K. It can be seen that the effective EAC increases with the increase of the particle diameter at the beginning and then approaches to a specific value. This variation trend of the EAC is similar to that of the EAC between the noble gases and the carbon nanotubes obtained by [Lin and McGaughey (2013)]. The reason may be that when a gas molecule moves into the action range of the nanoparticle, the bigger the particle size is, the much more atoms can interact with the gas molecule. Figure 13 is a schematic diagram of the interaction between a nanoparticle and a gas molecule.

In which, R is the radius of a nanoparticle and Rc is the cut-off radius of the interatomic potential between the particle and the gas. The region A includes the atoms belonging to the particle that can interact with the gas molecule and the region (A + B) includes the atoms belonging to the surface that can interact with the gas molecule. Obviously, the atoms in region A are less than that in the region (A + B) and as the diameter of the particle increases, the former approaches to the latter. Therefore, the EAC between a gas and a nanoparticle would approaches to the EAC between a gas and a surface as the particle size increases. Figure 14 shows the dependence of the ATC between the heat source and the heat sink versus the diameter of the particle with the same preset temperature, 300 K. The variation trend is similar to that of the EAC in Figure 12. Because the EAC is the main factor affecting the heat transfer rate when the collision rate keeps constant or changes slightly.

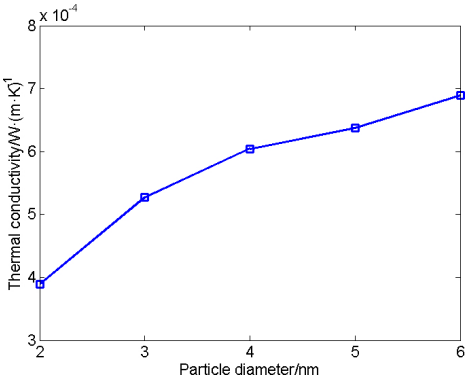

Figure 14: Dependence of ATC versus the nanoparticle diameter.

3.3 Results of different gas molecules

Table 5 listed the calculated EAC and ATC for the gases of Ar, N_2 and O_2 on a nanoparticle with the particle diameter 4 nm and the preset temperature 300 K. It can be seen that the EAC for the N_2 gas and the O_2 gas is close to each other and less than that of the Ar gas. In reference [Liang and Keblinski (2014)], the predicted EAC for the N_2 gas is also less than that of the Ar gas. However, the ATC

Table 5: Calculated results of different molecule types.

Molecule type	Ar	N_2	O_2
EAC	0.84 ± 0.05	0.34 ± 0.02	0.31 ± 0.03
ATC/W·(m·K)$^{-1}$	6.044×10^{-4}	6.2165×10^{-4}	6.6787×10^{-4}

for the three gases is close to each other. The reason is that, although the EAC for the Ar gas is bigger than that of the N_2 gas and the O_2 gas, the energy carried by a monatomic molecule (Ar) is smaller than that carried by a diatomic molecule (N_2, O_2).

4 Conclusions

The amorphous silica nanoparticles were generated using the melting-quenching process based on the MD simulations. The interaction between the gases and the nanoparticles were studied by the NEMD simulations. The effects of the temperature, the particle diameter and the molecule typeon the interaction were investigated.

The predicted EAC are all less than unity and decrease with the increase of the temperature which is in agreement with the experimental results in the literatures. For a fixed preset temperature, the EAC increases with the increase of the particle diameter at the beginning and eventually approaches to a specific value. The reason may be that when a gas molecule moves into the action range of the nanoparticle, more particle atoms can interact with the gas molecule with a bigger the particle size. With the same preset temperature, 300 K and the same particle diameter, 4 nm, the calculated EAC for the gases Ar, N_2 and O_2 are 0.84 ± 0.05, 0.34 ± 0.02 and 0.31 ± 0.03, respectively.

Because the distance between the heat source and heat sink is far less than the MFP of the gas molecules in free space and the EAC is less than unity, the predicted ATC is on the order of magnitudes of 10^{-4} $W \cdot (m \cdot K)^{-1}$ which is far less than the thermal conductivity of the gas in free space. It is also far less than the thermal conductivity through the interconnected nanoparticles composed the silica aerogels, which means that the heat transferred through the gas-nanoparticle interface is far less than the heat transferred through the neighbouring nanoparticles in silica aerogels.

References

Aegerter, M. A.; Leventis, N.; Koebel M. M. (2011): *Aerogels Handbook*. Springer.

Allen, M. P.; Tildesley D. J. (1987): *Computer Simulation of Liquids*. Clarendon Press.

Borisov, S.; Litvinenko S.; Semenov Y.; Suetin P. (1978): Experimental investigation of the temperature dependence of the accommodation coefficients for the

gases He, Ne, Ar, Xe on a Pt surface. *J. Eng. Phys. Thermophys*, vol. 34, pp. 603–606.

Chen, G. (2005): *Nanoscale energy transport and conversion A Parallel Treatment of Electrons, phonons, and Photons*. Oxford University Press.

Choi, M. S.; Yi, M. Y.; Lee, K. H.; Lee, J. W. (2012): Molecular-dynamics simulations of thermal accommodation of helium gas on a nanoparticle. *J. aerosol sci.*, vol. 44, pp. 62–70.

Coquard, R.; Baillis, D.; Grigorova, V.; Enguehard, F.; Quenard, D.; Levitz, P. (2013): Modelling of the conductive heat transfer through nano-structured porous silica materials. *J. Non-Cryst. Solids*, vol. 363, pp.103–115.

Dorcheh, A. S.; Abbasi, M. H. (2008): Review Silica aerogels; synthesis, properties and characterization. *J. Mater. Process. Technol.*, vol. 199, pp. 10–26.

Frenkel, D.; Smit, B. (2002): *Understanding Molecular Simulation from Algorithms to Applications*, Academic Press.

Fricke, J.; Heinemann, U.; Ebert, H. P. (2008): Vacuum insulation panels-from research to market. *Vacuum*, vol. 82, pp. 680–690.

Goodman, F. O.; Wachman, H. Y. (1976): *Dynamics of gas-surface scattering*, Academic Press.

Hoover, W. G. (1985): Canonical dynamics: Equilibrium phase-space distributions. *Phys. Rev. Appl*, vol. 31, no. 3, pp. 1965–1967.

Huang, Z. X.; Tang, Z. A.; Yu, J.; Bai, S. Y. (2009): Thermal conductivity of amorphous and crystalline thin films by molecular dynamics simulation. *Physica B*, vol. 404, pp. 1790–1793.

Jund, P.; Jullien, R. (1999): Molecular-dynamics calculation of the thermal conductivity of vitreous silica. *Phys. Rev. B*, vol. 59, no. 21, pp. 13707–13711.

Kittel, C. (2005): *Introduction to Solid State Physics*. John Wiley.

Lin, H.; McGaughey, A. J. H. (2013): Energy accommodation between noble gases and carbon nanotubes. *J. Phys. Chem. C*, vol. 117, pp. 18804–18808.

Liang, Z.; Evans, W.; Desai, T.; Keblinski, P. (2013): Improvement of heat transfer efficiency at solid-gas interfaces by self-assembled monolayers. *Appl. Phys. Lett.*, vol. 102, pp. 061907-1–061907-5.

Liang, Z.; Evans, W.; Keblinski, P. (2013): Equilibrium and nonequilibrium molecular dynamics simulations of thermal conductance at solid-gas interfaces. *Phys. Rev. E*, vol. 87, pp. 022119-1–022119-7.

Liang, Z.; Keblinski, P. (2014): Parametric studies of the thermal and momentum accommodation of monatomic and diatomic gases on solid surfaces. *Int. J. Heat Mass Transfer*, vol. 178, pp. 61–169.

Mahajan, S. S.; Subbarayan, G. (2007): Estimating thermal conductivity of amorphous silica nanoparticles and nanowires using molecular dynamics simulations. *Phys. Rev. E*, vol. 76, 056701-1–056701-14.

Malek, K.; Sahimi, M. (2012): Molecular dynamics simulations of adsorption and diffusion of gases in silicon-carbide nanotubes. *J. Chem. Phys.*, vol. 132, pp. 014310-1–014310-10.

Namilae, S.; Chandra, U.; Srinivasan, A.; Chandra, N. (2007): Effect of interface modification on the mechanical behavior of carbon nanotube reinforced composites using parallel molecular dynamics simulations. *CMES: Computer Modeling in Engineering & Sciences*, vol. 22, no. 3, pp. 189–202.

Nasrabadi, A. T.; Foroutan, M. (2012): Air adsorption and separation on carbon nanotube bundles from molecular dynamics simulations. *Comput. Mater. Sci.*, vol. 61, pp. 134–139.

Nosé, S. (1984): A unified formulation of the constant temperature molecular dynamics methods. *J. Chem. Phys.*, vol. 81, pp. 511–519.

Plimpton, S. (1995): Fast parallel algorithms for short-range molecular dynamics. *J. Comput. Phys.*, vol. 117, pp. 1–19.

Schiffres, S. N.; Kim, K. H.; Hu, L.; McGaughey, A. J. H; Islam, M. F.; Malen, J. A. (2012): Gas diffusion, energy transport, and thermal accommodation in single-walled carbon nanotube aerogels. *Adv. Funct. Mater.*, vol. 22, pp. 5251–5258.

Su, G. H; Yang, Z. C.; Sun, F. R. (2014): Molecular dynamics simulation of thermal conductivity of primary particle of silica aerogels. *J. Mech. Eng.*, vol. 50, no. 3, pp. 178–185.

Sun, J.; Li, Z. X. (2009): Molecular dynamics simulations of energy accommodation coefficients for gas flows in nano-channels. *Mol. Simul.*, vol. 35, no. 3, pp. 228–233.

Thomas, C.; Jin, F.; Laurent, P. (2011): Molecular dynamic study of thermal conductivity of amorphous nanoporous silica. *Int. J. Heat Mass Transfer*, vol. 54, pp. 4540–4548.

Touloukian, Y. S. (1970): Thermophysical properties of matter. IFI/Plenum.

Tu, Q. S.; Lee, M.; Zhang, S.; Li, S. F. (2014): Molecular dynamics simulations of ions diffusion in carbon nanotubes embedded in cell membrane. *CMES: Computer Modeling in Engineering & Sciences*, vol. 98, no. 3, pp. 247–259.

Van Beest, B. W. H.; Kramer, G. J.; Van Santen, R. A. (1990): Force fields for silicas and aluminophosphates based on ab initio calculations. *Phys. Rev. Lett.*, vol. 64, no. 16, pp. 1955–1958.

Wolf, D.; Keblinski, P.; Phillpot, S. R.; Eggebrecht, J. (1999): Exact method for the simulation of coulombic systems by spherically truncated, pairwise r^{-1} summation. *J. Chem. Phys.*, vol. 110, no. 17, pp. 8254–8282.

Yoon, Y. G.; Car, R. B.; Srolovitz, D. J. (2004): Thermal conductivity of crystalline quartz from classical simulations. *Phys. Rev. B*, vol. 70, pp. 012302-1–012302-1-4.

Yoshioka, T.; Asaeda, M.; Tsuru, T. (2007): A molecular dynamics simulation of pressure-driven gas permeation in a micropore potential field on silica membranes. *J. Membr. Sci.*, vol. 293, pp. 81–93.

Zhang, Z. M. (2007): *Nano/microscale heat transfer*, McGraw-Hill.